Journal Pre-proof

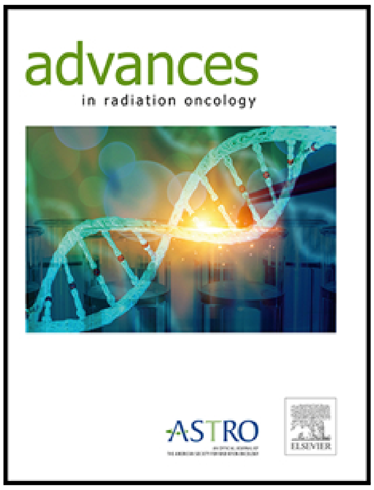

MRI-based delineation of organs at risk in the head and neck region

Viktor R. Paczona , Marta E. Capala , Borbála Deák-Karancsi , Emőke Borzási , Zoltán Végváry , Gyöngyi Kelemen , Renáta Kószó , László Ruskó , Lehel Ferenczi , Gerda M. Verduijn , Steven F. Petit , Judit Oláh , Adrienne Cserháti , Florian Wiesinger , Katalin Hideghéty

PII: S2452-1094(22)00148-8
DOI: https://doi.org/10.1016/j.adro.2022.101042
Reference: ADRO 101042

To appear in: *Advances in Radiation Oncology*

Received date: 20 April 2022
Accepted date: 24 July 2022

Please cite this article as: Viktor R. Paczona , Marta E. Capala , Borbála Deák-Karancsi , Emőke Borzási , Zoltán Végváry , Gyöngyi Kelemen , Renáta Kószó , László Ruskó , Lehel Ferenczi , Gerda M. Verduijn , Steven F. Petit , Judit Oláh , Adrienne Cserháti , Florian Wiesinger , Katalin Hideghéty , MRI-based delineation of organs at risk in the head and neck region, *Advances in Radiation Oncology* (2022), doi: https://doi.org/10.1016/j.adro.2022.101042

MRI-based delineation of organs at risk in the head and neck region
MR-only delineation in the H&N region

Viktor R. Paczona [1], Marta E. Capala [3], Borbála Deák-Karancsi [2], Emőke Borzási [1], Zoltán Végváry [1], Gyöngyi Kelemen [1], Renáta Kószó [1], László Ruskó [2], Lehel Ferenczi [2], , Gerda M. Verduijn [3], Steven F. Petit [3], Judit Oláh [1], Adrienne Cserháti [1] Florian Wiesinger [4] and Katalin Hideghéty [1,5]
[1]University of Szeged, Department of Oncotherapy
[2]GE Healthcare Hungary Kft.
[3]Erasmus MC Cancer Insitute
[4]GE Healthcare Munich, Germany
[5]ELI-HU Non-Profit Ltd.
Corresponding Author: Name: Viktor Róbert Paczona MD, **E-mail address:** paczona.viktor.robert@med.u-szeged.hu (Phone: 003630/4946436)
Author Responsible for Statistical Analysis: N/A

Conflict of Interest
None

Funding
This research is part of the Deep MR-only Radiation Therapy activity (project numbers: 19037, 20648, 210995) that has received funding from EIT Health. EIT Health is supported by the European Institute of Innovation and Technology (EIT), a body of the European Union receives support from the European Union´s Horizon 2020 Research and innovation program.

Data Availability Statement for this Work
Research data are stored in an institutional repository and will be shared upon request to the corresponding author.

Abstract

Background: The aim of this paper is to establish a comprehensive contouring guideline for treatment planning using only MR images through an up-to-date set of organs at risk (OAR), recommended organ boundaries and relevant suggestions for the MRI based delineation of OARs in the head and neck (H&N) region.

Materials and Methods: After a detailed review of literature MRI data were collected from the H&N region of healthy volunteers. OARs were delineated in the axial, coronal, and sagittal planes on T2 weighted sequences. Every contour defined has been revised by four radiation oncologists and subsequently, by two independent senior experts, a H&N radiation oncologist and a radiologist. After revision, the final structures were presented to the consortium partners.

Results: Definitive consensus was reached after multi-institutional review. On that basis we have provided detailed anatomical and functional description and specific MRI characteristics of the OARs

Conclusions: In the era of precision radiotherapy, the need for well-built, straightforward contouring guidelines is on the rise. Precise, uniform delineation based automatized OAR segmentation on MR imaging may lead to increased accuracy in terms of organ boundaries, and analysis of dose dependent sequelae for adequate definition of the normal tissue complication probability.

1. Introduction

Accurate organ at risk (OAR) delineation in the era of precision radiotherapy (RT) is essential for the irradiation of head and neck (H&N) cancer. Both postoperative and definitive organ-preserving radiotherapy with or without chemotherapy are widely applied in the complex management of this disease. While radiotherapy is highly effective in the treatment of cancer a substantial rate of serious acute side effects and often severe, treatment-related late toxicities occur. Acute mucositis during dose delivery as well as late functional damages of healthy organs may lead to xerostomia and swallowing difficulties, significantly deteriorating the quality of life of the patients. Consistent definition and delineation of OARs using highly selective, conformal plans is vital in order to spare normal structures.

Both traditionally and at present, the generally used imaging method for contouring purposes is computed tomography (CT). A consensus guideline [1] was published in 2015 on CT-based OAR delineation for the H&N region. The hegemony of CT is, however, challenged by newly emerged, advanced methods that provide detailed images with far superior soft tissue resolution in comparison to computed tomography (magnetic resonance imaging; MRI, [2; 3]).

MRI-only treatment planning has several clinical advantages, such as the avoidance of multiple imaging processes and exposure to ionizing radiation during imaging. The latter has a greater relevance if repeated imaging is applied for replanning purposes during adaptive radiotherapy.

In the meantime, MRI-only based contouring has a number of drawbacks as well. Due to the more complex physical background, selecting and interpreting the adequate sequences require more experience. Moreover, getting to know the specific MRI characteristics of the given OARs may take a longer time and more practice. In the future, thanks to automated organ at risk delineation, this learning process will become needless and errors due to human mistakes will be less likely to occur.

It is with the availability of such modalities, that the need for a large number of accurate OAR contours in the head and neck region, including subunits of larger organs and organelles, can be satisfied. Although magnetic resonance imaging has long been used for tumor delineation, its implication in organ at risk contouring remains a question of debate [4-6].

Since 2015 many publications have appeared, focusing on new potential organs at risk in the anatomical region at hand. As a result of this process, numerous different sets of OARs coexist, in some cases accompanied by MRI based contouring atlases.

The purpose of this paper is to establish a comprehensive contouring guideline for treatment planning using only MR images through an up-to-date set of OARs, recommended organ boundaries and relevant suggestions of the MRI based delineation of organs at risk.

2. Materials and Methods

The ongoing project: XXXX aims to develop a software that can provide automatic OAR contours on MR images [7]. The first phase of development required numerous precise, manually contoured expert cases. During the project, the need emerged for definition of MRI acquisition techniques and delineation of OARs in the head and neck region on MR images.

To that aim, the technical details of MRI acquisition for treatment planning, reasonably required MRI sequences and an up-to-date set of OARs were defined, relying on the latest existing guidelines [1; 8-14]. The method comprised of a systematic review of the latest publications and discussions for consensus in the divergent points by the representatives of the participating institutions.

The next step was MRI data collection from the head and neck region of 7 healthy volunteers in diagnostic setting (supine position, dedicated Head/Neck coil, as detailed in Table 1). The OARs were delineated using the ECLIPSE treatment planning system (Varian Medical Systems, version: 13.6) in the axial, coronal and sagittal planes on T2 weighted sequences. Every contour defined has been revised by four radiation oncologists and subsequently, by two independent senior experts, a head and neck radiation oncologist and a radiologist. Following this two-step revision, the final structures were presented to the consortium partners in Rotterdam. Definitive consensus was reached after multi-institutional review. In order to visualize our findings and suggestions, we have compiled an atlas containing an expert case, which can be found in the supplementary materials section.

MR imaging for OAR delineation was based on 2D and 3D T2-weighted fast spin echo (FSE) sequences with sufficient geometric coverage to include all relevant OARs (i.e., top of the head to the middle of the neck). More specifically, the T2 FSE sequences included 2D fast-recovery FSE (frFSE), 2D PROPELLER^{TM}, and 3D CUBE^{TM}. Detailed sequence parameters are outlined in Table 1.

From the point of view of tissue contrast, no significant differences were found between the tested sequences. However 2D sequences are more sensitive to patient motion (swallowing, eye movements) and thus imaging artifacts are more likely to occur. This is the main reason why the volunteer scan included in the atlas is a 3D Sagittal T2 CUBE sequence, though our contouring atlas is applicable to any diagnostic T2 weighted MRI sequence. The reconstruction diameter was 350 mm, the pixel size 0.664 mm and the spacing-between-slices 0.5 mm. The selection criteria for the atlas case included high resolution, good contrast and lack of imaging artifacts. Prior to manual contouring, the original scan was reformatted to axial orientation and isotropic voxel size (0.664 mm) using Volume Viewer application of Advantage Workstation 4.7 to make it compatible with all radiation therapy planning software. Our choice of MRI sequence relied on a scoring table (Table 6.), in which the visibility of the organs at risk was evaluated on T1 and T2 weighted MRI sequences, as well as on CT. The most important aspects of evaluation were sharpness of margins and demarcation from the surrounding tissues. A scale ranging from 1 to 3 was utilized, where 3 stood for excellent, 2 for average and 1 for poor visibility. Based on the results of this evaluation, we have found that T2 weighted MRI sequences are more suitable for OAR delineation than T1 ones.

In addition to organ contouring, the MR-only radiation therapy planning requires synthetic CT to enable dose calculation. The technical feasibility of the MR-based synthetic CT was already demonstrated by several studies [15; 16].

3. Results

We summarized here our findings during the contouring session as well as the recommended OAR boundaries. Table 6. also contains useful information on the MRI characteristics of the different OARs by the end of this section.

3.1. Parotid glands

The parotid gland is the largest of the major salivary glands, approximately 55-60 mm in craniocaudal and 30-35 mm in anteroposterior dimension [8]. It is composed of an inverted triangle-shaped superficial and a deep lobe, located behind the ramus of the mandible. A number of important vessels and nerves pass through the gland. The facial nerve pierces its substance in postero-anterior direction; this can be regarded as the border between the superficial and deep lobes. Deep to the facial nerve passes the external carotid artery to terminate as two branches inside the parotid gland: maxillary and superficial temporal artery. Superficial to the arteries are the superficial temporal and maxillary veins, joining to form the retromandibular vein.

3.1.1. Contouring suggestions:

- The delineation of the external carotid artery and retromandibular vein was carried out in a few cases in order to precisely define the medial border of the organ and to distinguish between the vessels and the styloid process, as well as the muscles arising from the latter.
- An accessory parotid gland is sometimes present alongside the parotid duct, on the outer surface of the masseteric muscle that has to be included in the contour.
- Fatty infiltration/replacement of the secretory tissue may be present at older ages, which may make the outline of the organ more difficult to define [17]. This may also arise as a therapeutic side effect of previous irradiation.
- See Table 2. for the recommended anatomical boundaries.

3.2. Submandibular glands

The largest portion of the walnut-sized (approximately 27 mm in length and 13-14 mm in width) submandibular gland lies in the submandibular triangle, and usually exceeds the level of the inferior border of the mandibular corpus (i.e. the cranial border of the submandibular triangle) in the cranial direction. Inferiorly, it reaches the insertion of the stylohyoid muscle (body and greater horn of hyoid bone) and the intermediate tendon of the digastricus. A tongue like extension of the gland, often referred to as the deep process, arises from the medial surface of the gland and spreads above the mylohyoid muscle. The facial artery leads a tortuous path, which passes through the medial part of the organ, while the facial vein is situated on the superficial surface.

3.2.1. Contouring suggestions:

- See Table 2. for the recommended anatomical boundaries.

3.3. Mandible

The mandible, or jawbone consists of a parabolic-shaped body that is connected by a right and left ramus to the rest of the cranium. The two rami terminate in the condyles, which form the articular head of the temporomandibular joints.

3.3.1. Contouring suggestions:

- The alveoli or teeth sockets of the mandibular corpus are still included in the contour, but not the teeth.
- We have omitted the coronoid process from the contour since its cranial border is hard to define univocally on axial MRI slices and radiation necrosis affects primarily the body [18].

3.4. Supraglottic larynx

The upper part of the larynx is composed of the epiglottis, the aryepiglottic folds, the false vocal or vestibular cords, the arytenoid cartilages and the mucosa coating them. Charlotte L. Brouwer et al. [1] defined the inferior border of the supraglottis as the cranial edge of arytenoid cartilages. This, however, contradicts the fact that the vestibular cords form an integral part of the supraglottic larynx, since their origin and insertion (anter-olateral surface of the arytenoid cartilage, just above the vocal process – angle of thyroid cartilage, below the attachment of the epiglottis) is situated below the apex of the arytenoids. The pyriform sinus shall be excluded from the contour, as it belongs to the hypopharynx.

3.5. Glottic larynx/glottic area

The glottic larynx is an anatomical subsite of the larynx, below the supraglottis, and above the subglottis. The name of the area is derived from the glottis, the gap between the true vocal cords. According to the 7th edition of AJCC Cancer Staging Manual [19], the glottis contains the true vocal cords, including its anterior and posterior commissures. The overall thickness of the structure is approximately 10 mm in the horizontal plane.

3.5.1. Contouring suggestions:

- See Table 3. for the recommended anatomical boundaries of the laryngeal structures.

3.6. Oral cavity

Opposite to the previously enumerated structures, the oral cavity is not an organ on its own, but an anatomical area within the mouth that is located anterior to the oropharynx [20]. Its contour includes the hard and soft palate as well as the lingual tonsils, since their mucosa must be spared from an excessive dose of ionising radiation. This consideration led us to an OAR contour that is somewhat larger than the oral cavity proper (i.e., the cavity behind the dental arches, excluding the oral vestibule between the lips and teeth).

3.6.1. Contouring suggestions:

- See Table 3. for the recommended anatomical boundaries.

3.7. Pharyngeal constrictor muscles (PCMs)

The muscles of the pharynx can be divided into an outer circular and an inner longitudinal layer. The former includes the superior (superior constrictor; SC), middle (middle constrictor; MC) and inferior (inferior constrictor; IC) pharyngeal constrictor muscles, responsible for propelling the bolus into the esophagus.

3.7.1. Contouring suggestions:

- Apart from the PCMs, various other structures play an indispensable role in the process of swallowing. These structures are the muscles of the floor of the mouth (the anterior belly of digastric muscle, mylohyoid and geniohyoid muscle), the thyrohyoid muscle, the posterior digastric/stylohyoid muscle complex, the longitudinal pair of the pharyngeal constrictors i.e. the longitudinal pharyngeal muscles (LCMs), the hyoglossus/styloglossus complex, the genioglossus muscle and, finally, the muscles responsible for tongue motion; the intrinsic tongue muscles, which are referred to collectively as functional swallowing units (abbreviated as FSUs [9; 21]). The three major physiological roles of these structures are tongue motion, tongue base retraction and hyolaryngeal elevation. The usefulness of FSU delineation in daily routine is a source of debate, due to the extreme workload demand and eventual overlaps with other sensitive areas, such as the oral cavity and certain laryngeal structures. The contouring process might be facilitated in some cases by the usage of automatic OAR segmentation, as stated in the article of the MD Anderson Head and Neck Cancer Symptom Working Group [22]. To the best of our knowledge, neither dose constraints, nor exact fields of implication have been defined for these structures.

- See Table 4. for the recommended anatomical boundaries.

3.8. Inner ear

The inner ear is comprised of two main functional parts, the cochlea, and the vestibular system. They consist of an outer bony labyrinth, a network of passages with bony walls within the petrous part of the temporal bone and an inner fluid-filled membranous labyrinth. The cochlea is a spiraled tunnel that makes 2¾ turns about its axis, the modiolus, which is perpendicular to the longitudinal axis of the petrous bone. The semicircular canals are situated posterolaterally to the cochlea and are made up of three tubes according to the three main planes of space, interconnected by a central vestibule [26].

<u>3.8.1. Contouring suggestions:</u>

- The cochlea and vestibular system have been delineated separately in some cases. However, due to the proximity of the two structures, we have defined the inner ear as one single OAR, following the practice of Sun et al. [27].

3.9. Eye (eyeball)

The eyeball consists of three outer tunics (sclera, choroid, and retina) encompassing the core of the eye itself. This can be subdivided into four further anatomical structures, the anterior & posterior chambers, lens, and vitreous body. Finer microscopic anatomical details, however, cannot be observed on MRI scans.

<u>3.9.1. Contouring suggestions:</u>

- A meticulous delineation of the fluid filling the anterior chamber and the vitreous body can be carried out. The extension of this contour by 1 mm (corresponding to the outer layers of the eye) in all dimensions may also lead us to an adequate OAR contour.

3.10. Lens

The lens of the eye is a biconvex, lentiform structure suspended between the iris and vitreous body. Its overall diameter typically ranges between 9 and 10 mm, with a thickness of approximately 4,5 mm, though this varies with age.

3.11. Optic nerve

Also known as cranial nerve II, the optic nerve is composed of ganglion cell axons that carry the excitation of retinal photoreceptors to the vision centers of the cortex. The orbital portion of the nerve is usually between 20 and 30 mm in length and 2-5 mm in thickness. It travels in the axis of the orbit, above the rectus inferior muscle and below the rectus superior. It enters the cranial cavity via the optic canal to terminate in the optic chiasm. The intracranial segment of the optic nerve is approximately 10 mm long.

<u>3.11.1. Contouring suggestions:</u>

- The optic nerve can be confused for the rectus superior and inferior muscles. The muscles have a flat, shorter appearance, while the nerve is slimmer and longer.
- The meningeal layers ensheathing the nerve have also been included in the contour.

3.12. Optic chiasm

The optic chiasm is the location of the partial decussation of optic fibers. It rests upon the tuberculum sellae, in the suprasellar cistern. The crossing fibers form an X-shape, posteriorly bordered by the pituitary stalk, laterally by the internal carotid arteries and inferiorly by the third ventricle. The circle of Willis encircles the pituitary stalk and optic chiasm. The overall size of the structure is usually 14 x 8 x 5 mm [10].

<u>3.12.1. Contouring suggestions:</u>

- The X-shape is not always visible on one single section, especially when operating with small slice thickness (1 mm or below). In such cases, the fibers of the optic nerve entering the chiasma and the axons forming the optic tract can be delineated on consecutive MRI slices.
- The pituitary stalk and internal carotid arteries may additionally be delineated to help distinguish between the chiasm and the surrounding structures.

3.13. Lacrimal gland

The lacrimal gland is a small exocrine gland that is situated in a shallow depression of the superolateral corner of the orbit.

3.13.1. Contouring suggestions:

- The easiest way to find the gland is to look for an approximately 15 x 20 x 5 mm area with low signal intensity, above the lateral rectus muscle and laterally to the superior rectus muscle [28].
- The volume of the lacrimal gland is usually around 0.6 cm^3 with a slight right-sided dominance [29; 30].

3.14. Brainstem

The rostral continuation of the spinal cord can be subdivided into three levels in rostro-caudal order. The lowermost one-third, the medulla oblongata has no well-determined inferior border since transition from the spinal cord to the brainstem is continuous. To overcome this uncertainty, we have commenced the contouring of the medulla at the level where the tip of the odontoid process first appears, in concordance with CT based guidelines [1]. The rostral limit of the mesencephalon, or midbrain (the uppermost third of the brainstem) is similarly ill-defined. A recent study carried out on OAR contouring in the central nervous system using MRI technique suggests to delineate the midbrain till the disappearance of the nigral substance [10]. The previously mentioned CT based consensus guideline defines the cranial beginning of the midbrain as the bottom section of the lateral ventricles. We do not entirely agree with this approach, since the temporal horns of the lateral ventricles appear already at the level of the ponto-mesencephalic junction, therefore more caudally than the expected organ margin. We have found that the central part of the lateral ventricle is a more reliable landmark for the upper border of the mesencephalon. Another study by Beddok et al. [11] suggests to place the brainstem between the uppermost and lowermost endpoints of the Sylvian aqueduct, a CSF filled narrow cavity that is well visible in the sagittal plane.

3.14.1. Contouring suggestions:

- The average volume of the brainstem is expected to fall between 27 and 43 cm^3 [31].

3.15. Spinal cord

The spinal cord is the caudal continuation of the brainstem, extending from the lowermost section of the medulla to the intervertebral disc between the first and second lumbar vertebrae.

3.16. Brain

Our brain contour includes the brainstem, diencephalon, cerebellum, hemispheria of the telencephalon, smaller cerebral vessels, and the cerebrospinal fluid. Since our approach treats the brainstem as a subunit of the OAR brain, the lowermost section of these two is located in an identical plane.

3.16.1. Contouring suggestions:

- The contouring of this organ mainly involves following the outline cerebrospinal fluid in the subarachnoid space.

3.17. Pituitary gland

The pituitary gland, or hypophysis, is a cherry-sized endocrine organ located within the cranial cavity. It can be regarded as a caudal protrusion of the hypothalamus, connected by the pituitary stalk to the latter.

3.17.1. Contouring suggestions:

- The hypophysis rests in a small, saddle-shaped bony nest of the sphenoid bone, the sella turcica. The organ itself is usually well visible on any diagnostic T2 weighted MRI sequences, though the sella itself is difficult to find. On CT scans with appropriate bone window, we can localize the clinoid processes, the dorsum and the tuberculum sellae, important anatomical landmarks bordering the hypophyseal fossa, and thus, the hypophysis.

3.18. Thyroid gland

The thyroid gland is an endocrine organ that lies against and around the thyroid and cricoid cartilages of the larynx. It is made up of two elongated lobes interconnected by a narrow isthmus, giving the thyroids the shape of a butterfly. The size of the lobes may vary on a wide range, but the average antero-posterior diameter of the organ falls usually between 13 and 28 mms, with a length of 40-60 mm. The volume of the OAR is 12-18 ml in the male and 10-15 ml in the female population [32; 33].

3.19. Brachial plexus (BP)

The brachial plexus is a network of nerves that provides sensory and motor innervation of the upper limb and shoulder girth. The course of the plexus can be divided into four distinct portions, each related to characteristic anatomical landmarks. The first portion, i.e. the radices or roots of the brachial plexus correspond to the anterior rami of C5-T1 spinal nerves. These roots later merge to form the superior, middle and inferior trunks of the plexus, which are situated above the clavicle, in the scalene hiatus. Behind the clavicle, each trunk splits in two, forming a total of six divisions. The last portion of the brachial plexus are the cords, located below the clavicle, in the axillary fossa. They are named by their position with respect to the axillary artery. The recommended anatomical boundaries for the brachial plexus are included in Table 5.

3.20. Esophagus

Starting at the level of the sixth cervical vertebra, the thumb-thick foodpipe interconnects the pharynx with the cardia of the stomach. It rests on the vertebral bodies, just behind the larynx and the trachea.

3.20.1. Contouring suggestions:

- Between the ventral trachea and the dorsal esophagus runs the shallow trache-oesophageal groove, which contains the recurrent laryngeal nerve. The sparing of this nerve may be desirable in order to prevent late-onset radiation induced neuropathy [37; 38].

4. Discussion

The role of novel anatomical structures and subsites as potential organs at risk emerges, just as we have seen in the case of the masticatory muscles [45] or the freshly described tubarial salivary glands [46]. With the growing number of clinical trials requiring MRI based radiation therapy planning, the need for well-built, straightforward contouring guidelines [47; 48]. is on the rise. Automatized OAR segmentation (not only in the head and neck region) combined with MRI based imaging may lead to increased accuracy in terms of organ boundaries and decreased interobserver variability [49; 50]. Generally speaking, the rapid evolution of artificial intelligence (AI) based contouring software may take a huge burden off the shoulders of radiographists and radiation oncologists and may result in the expansion of this proposed organ set. OAR delineation should always be governed by clinical rationality that takes into account the stage of the disease, tumor volume and involvement/infiltration of different anatomical structures, functional units, as well as the curative or palliative intent of the radiotherapy itself.

5. Conclusions

Within the framework of cooperation between several European clinical centers, a consensus guideline was established on OAR delineation in the head and neck region, using exclusively MR images. Such uniform guidelines may increase treatment accuracy and facilitate the comparison of results between different centers, collaborations and multi-institutional clinical trials.

Declaration of interests

The authors declare the following financial interests/personal relationships which may be considered as potential competing interests:

References

1. Charlotte L. Brouwer, Roel J.H.M. Steenbakkers et al.: CT-based delineation of organs at risk in the head and neck region: DAHANCA, EORTC, GORTEC, HKNPCSG, NCIC CTG, NCRI, NRG Oncology and TROG consensus guidelines. *Radiotherapy and Oncology.* 2015; 117: 83-90
2. G. Widmann, B. Henninger et al.: MRI Sequences in Head & Neck Radiology – State of the Art. *Fortschritte auf dem Gebiete der Röntgenstrahlen und der Nuklearmedizin.* 2017; 189: 413-422
3. Y.L. Dai, A.D. King.: State of the art MRI in head and neck cancer. *Clinical Radiology.* 2018; 73: 45-59
4. Jelena Lukovic, Lauren Henke et al.: MRI-Based Upper Abdominal Organs-at-Risk Atlas for Radiation Oncology. *International Journal of Radiation Oncology, Biology, Physics.* 2020; 106: 743-753
5. C. Olsson, T. Nyholm et al.: Initial experience with introducing national guidelines for CT- and MRI-based delineation of organs at risk in radiotherapy. *Physics and Imaging in Radiation Oncology*. 2019; 11: 88-91

6. J. Yuan, O. Wong et al.: Delineation Variability of Head and Neck Organs at Risk on T1-Weighted Isotropic Magnetic Resonance Images: A Pilot Study on Healthy Volunteers. *International Journal of Radiation Oncology, Biology, Physics.* 2019; 96: E609
7. Laszlo Rusko, Bernadett Kolozsvari et al.: Automated organ delineation in T2 head MRI using combined 2D and 3D convolutional neural networks. *ESTRO.* 2020; DOI: 10.3252/pso.eu.ESTRO2020.2020
8. Frank Hoebers, Eugene Yu et al.: A pragmatic contouring guideline for salivary gland structures in head and neck radiation oncology: the MOIST target. *American Journal of Clinical Oncology-Cancer Clinical Trials.* 2013; 36: 70-76
9. Agata Gawryszuk, Hendrik P. Bijl et al.: Functional Swallowing Units (FSUs) as organs-at-risk for radiotherapy. PART 2: Advanced delineation guidelines for FSUs. *Radiotherapy and Oncology.* 2019; 130: 68-74
10. Danielle BP Eekers, Lieke in ’t Ven et al.: The EPTN consensus-based atlas for CT- and MR-based contouring in neuro-oncology. *Radiotherapy and Oncology.* 2018; 128: 37-43
11. Arnaud Beddok, Jean-Christophe Faivre et al.: Practical contouring guidelines with an MR-based atlas of brainstem structures involved in radiation-induced nausea and vomiting. *Radiotherapy and Oncology.* 2019; 130: 113-120
12. Abraham J. Wu, Walter R. Bosch et al.: Expert consensus contouring guidelines for IMRT in esophageal and gastroesophageal junction cancer. *International Journal of Radiation Oncology, Biology, Physics.* 2015; 92: 911-920
13. Miranda E. M. C. Christianen, Johannes A. Langendijk et al.: Delineation of organs at risk involved in swallowing for radiotherapy treatment planning. *Radiotherapy and Oncology.* 2011; 101: 394-402
14. Minh Tam Truong, Rohini N. Nadgir et al.: Brachial Plexus Contouring with CT and MR Imaging in Radiation Therapy Planning for Head and Neck Cancer. *RadioGraphics.* 2010; 30: 1095-1103

15. Florian Wiesinger, Mikael Bylund et al.: Zero TE-based pseudo-CT image conversion in the head and its application in PET/MR attenuation correction and MR-guided radiation therapy planning. *Magnetic Resonance in Medicine.* 2018; 80: 1440-1451
16. Paul Blanc-Durand, Maya Khalife et al.: Attenuation correction using 3D deep convolutional neural network for brain 18F-FDG PET/MR: Comparison with Atlas, ZTE and CT based attenuation correction. *PLoS One.* 2019; DOI: 10.1371/journal.pone.0223141
17. Davi SousaGarcia, Ivo Bussoloti Filho: Fat deposition of parotid glands. Brazilian *Journal of Otorhinolaryngology.* 2013; 79: 173-176
18. Ravindran Rathy, S. Sunil et al.: Osteoradionecrosis of mandible: Case report with review of literature. *Contemporary Clinical Dentistry.* 2013; 4: 251-253
19. Stephen B. Edge, April G. Fritz et al.: AJCC Cancer Staging Manual Seventh Edition. *Springer.* 2010
20. Daniel W. Williams III: An Imager's Guide to Normal Neck Anatomy. *Seminars in Ultrasound, CT and MRI.* 1997; 18: 157-181
21. Agata Gawryszuk, Hendrik P. Bijl et al.: Functional Swallowing Units (FSUs) as organs-at-risk for radiotherapy. PART 1: Physiology and anatomy. *Radiotherapy and Oncology.* 2019; 130: 62-67
22. MD Anderson Head and Neck Cancer Symptom Working Group: Beyond mean pharyngeal constrictor dose for beam path toxicity in non-target swallowing muscles: dose-volume correlates of chronic radiation-associated dysphagia (RAD) after oropharyngeal intensity modulated radiotherapy. *Radiotherapy and Oncology.* 2016; 118: 304-314
23. Alfio Ferlito, Alessandra Rinaldo: The pathology and management of subglottic cancer. European Archives of Oto-Rhino-Laryngology 2000, Volume 257, 168-173
24. Piet Dirix, Sarah Abbeel et al.: Dysphagia After Chemoradiotherapy for Head-and-Neck Squamous Cell Carcinoma: Dose–Effect Relationships for the Swallowing

Structures. International Journal of Radiation Oncology, Biology, Physics 2009, Volume 75, 385-392

25. Aron Popovtzer, Yue Cao et al.: Anatomical changes in the pharyngeal constrictors after chemoirradiation of head and neck cancer and their dose-effect relationships: MRI-based study. Radiotherapy and Oncology 2009, Volume 93, 510-515
26. Niranjan Bhandare, Andrew Jackson et al.: Radiation therapy and hearing loss. *International Journal of Radiation Oncology, Biology, Physics.* 2010; 76: S50-S57
27. Ying Sun, Xiao-Li Yu et al.: Recommendation for a contouring method and atlas of organs at risk in nasopharyngeal carcinoma patients receiving intensity-modulated radiotherapy. *Radiotherapy and Oncology.* 2014; 110: 390-397
28. S. Scoccianti, B. Detti et al.: Organs at risk in the brain and their dose-constraints in adults and in children: A radiation oncologist's guide for delineation in everyday practice. *Radiotherapy and Oncology.* 2015; 114: 230-238
29. Erdogan Bulbul, Alper Yazici et al.: Evaluation of Lacrimal Gland Dimensions and Volume in Turkish Population with Computed Tomography. *Journal of Clinical and Diagnostic Research.* 2016; 10: TC06-TC08
30. Ozgun Melike Gedar Totuk, Aybike Buse et al.: Evaluation of Lacrimal Gland Dimensions with MR Imaging in a Turkish Population Sample. *International Journal of Morphology.* 2018; 36: 1431-1438
31. Charles Mayo, Ellen Yorke et al.: Radiation associated brainstem injury. *International Journal of Radiation Oncology, Biology, Physics.* 2010; 76: S36-S41
32. Vikas Chaudhary and Shahina Bano: Thyroid ultrasound. *Indian Journal of Endocrinology and Metabolism.* 2013; 17: 219-227
33. Taewoo Kang, Dong Wook Kim et al.: Magnetic Resonance Imaging Features of Normal Thyroid Parenchyma and Incidental Diffuse Thyroid Disease: A Single-Center Study. *Frontiers in Endocrinology*. 2018; DOI: 10.3389/fendo.2018.00746
34. William H. Hall, Michael Guiou et al.: Development and Validation of a Standardized Method for Contouring the Brachial Plexus: Preliminary Dosimetric Analysis Among

Patients Treated With IMRT for Head-and-Neck Cancer. International Journal of Radiation Oncology, Biology, Physics 2008, Volume 72, 1362-1367

35. Sun K. Yi, William H. Hall et al.: Validating the RTOG-Endorsed Brachial Plexus Contouring Atlas: An Evaluation of Re-producibility Among Patients Treated by Intensity-Modulated Radiotherapy for Head-and-Neck Cancer. International Jour-nal of Radiation Oncology, Biology, Physics 2012, Volume 82, 1060-1064
36. Joris Van de Velde, Emmanuel Audenaert et al.: An Anatomically Validated Brachial Plexus Contouring Method for Intensity Modulated Radiation Therapy Planning. International Journal of Radiation Oncology, Biology, Physics 2013, Volume 87, 802-808
37. David Benjamin Shultz, Nicholas Trakul et al.: Vagal and recurrent laryngeal neuropathy following stereotactic radiation therapy in the chest. *Practical Radiation Oncology.* 2014; 4: 272-278
38. Pariyanan Jaruchinda, Somjin Jindavijak et al.: Radiation-related vocal fold palsy in patients with head and neck carcinoma. Journal of the Medical Association of Thailand. 2012; 95: S23-8
39. J. A. Castelijns, J. Doornbos et al.: MR imaging of the normal larynx. Journal of Computer Assisted Tomograph. 1985; 9: 919-925
40. Jamie A. Dean, Liam C. Welsh et al.: A novel method for delineation of oral mucosa for radiotherapy dose–response studies. Radiotherapy and Oncology. 2015; 115: 63-66
41. M. Adachi, T. Hosoya et al.: Evaluation of the substantia nigra in patients with Parkinsonian syndrome accomplished using multishot diffusion-weighted MR imaging. American Journal of Neuroradiology. 1999. 20: 1500–1506
42. M. Wada, L. Premoselli et al.: Determination of Accuracy in the Delineation of Spinal Cord and Canal/Thecal Sac on CT and MRI in Head and Neck Planning. International Journal of Radiation Oncology, Biology, Physics. 2006; Volume 66: S450
43. Stephanie E. Combs, Brigitta G. Baumert et al.: ESTRO ACROP guideline for target

volume delineation of skull base tumors. Radiotherapy and Oncology. 2021; 156: 80-94

44. Abraham J. Wu, Walter R. Bosch et al.: Expert consensus contouring guidelines for IMRT in esophageal and gastroesophageal junction cancer. International Journal of Radiation Oncology, Biology, Physics. 2015; 92: 911-920
45. Xiangguo Zhang, | Haihui Chen et al.: Technical note: Atlas-based Auto-segmentation of masticatory muscles for head and neck cancer radiotherapy. *Journal of Applied Clinical Medical Physics.* 2020; 21: 233-240
46. Matthijs H. Valstar, Bernadette S. de Bakker et al.: The tubarial salivary glands: A potential new organ at risk for radiotherapy. *Radiotherapy and Oncology.* 2021; 154: 292-298
47. Vincent Grégoire, Mererid Evans et al.: Delineation of the primary tumour Clinical Target Volumes (CTV-P) in laryngeal, hypopharyngeal, oropharyngeal and oral cavity squamous cell carcinoma: AIRO, CACA, DAHANCA, EORTC, GEORCC, GORTEC, HKNPCSG, HNCIG, IAG-KHT, LPRHHT, NCIC CTG, NCRI, NRG Oncology, PHNS, SBRT, SOMERA, SRO, SSHNO, TROG consensus guidelines. *Radiotherapy and Oncology.* 2018; 126: 3-24
48. Diana Lin, Kaitlyn Lapen et al.: A Systematic Review of Contouring Guidelines in Radiation Oncology: Analysis of Frequency, Methodology, and Delivery of Consensus Recommendations. *International Journal of Radiation Oncology, Biology, Physics.* 2020; 107: 827-835
49. Anantharaman Ayyalusamy, Subramani Vellaiyan et al.: Auto-segmentation of head and neck organs at risk in radiotherapy and its dependence on anatomic similarity. *Radiation Oncology Journal.* 2019; 37: 134-142
50. Nuo Tong, Shuiping Gou et al.: Fully automatic multi-organ segmentation for head and neck cancer radiotherapy using shape representation model constrained fully convolutional neural networks. *Medical Physics Journal.* 2018; 45: 4558-4567

Tables

Table 1. Scan parameters for the three T2-weighted sequences used for OAR delineation.

	2D T2 frFSE	**2D T2 PROPELLER**	**3D T2 CUBE**
MRI scanner model	GE DISCOVERY MR750w	GE SIGNA Artist	GE SIGNA Artist
RF receive coil array	AIR RT Head&Neck	GEM Head&Neck	GEM Head&Neck
B0 [T]	3	1.5	1.5
BW [kHz]	62.5	83.3	125
TR [ms]	11866	7624	2002
TE [ms]	99.3	87.3	76.6
ETL	22	26	100
Scan time [s]	332.6	229.1	259.0
Scan orientation	axial	axial	sagittal
FOV [mm^2]	300x300	300x300	340x340
AcqRes [mm^2]	1.04x1.04	1.04x1.04	1.18x1.18
InterpRes [mm^2]	0.59x0.59	0.59x0.59	0.66x.066
Dz [mm]	3	3	1
Nz	100	80	340

With B0 the main magnetic field strength, BW the bandwidth (pixel bandwith * rows), TR the repetition time, TE the echo time, ETL the echo train length, AcqRes the acquires resolution (reconstruction diameter/acquisition matrix), InterpRes the interpolated resolution (reconstruction diameter/rows), Dz the slice thickness, and Nz the number of slices.

Table 2. Anatomical borders of the salivary glands.

Organ boundaries	Parotid glands	Submandibular glands
Anterior	Masseteric muscle, mandibular ramus, pterygoid muscles	Posterior margin of mylohyoid muscle, with the deep process spreading above the mylohyoid muscle
Posterior	Sternocleidomastoid muscle and the posterior belly of the digastric muscle	Parapharyngeal space, great vessels of the neck
Medial	Styloid process, styloglossus, stylohyoid and stylopharyngeal muscles	Superior: lateral surface of hyoglossus and partly mylohyoid muscles Middle: lateral surface of styloglossus and stylohyoid muscles, digastric muscle Inferior: lateral surface of the body of hyoid bone, pharyngeal constrictor muscles
Lateral	Platysma, subcutaneous tissue	Superior: medial surface of medial pterygoid muscle Middle: medial surface of the body of the mandibular bone Inferior: platysma, investing layer of deep cervical fascia, fat tissue
Cranial	Superior wall of of the external auditory canal, mastoid process	Medial pterygoid muscle
Caudal	No distinct border, the organ gradually disappears in the fat tissue of the neck	No distinct border, the organ gradually disappears in the fat tissue of the neck

Table 3. Anatomical borders of the laryngeal structures and the oral cavity.

Organ boundaries	**Supraglottic larynx**	**Glottic larynx**	**Oral cavity**
Anterior	Hyoid bone, pre-epiglottic space, thyroid cartilage [1]	Thyroid angle	Inner surface of superior and inferior dental arches
Posterior	Posterior pharyngeal wall	Inner surface of cricoid and arytenoid cartilages	Posterior border of soft palate and uvula, root of the tongue [1]
Medial	NA (lumen of the larynx)		NA
Lateral	Inner surface of thyroid cartilage		Inner surface of dental arches, maxilla and mandible
Cranial	Tip of epiglottis [1]	Caudal boundary of supraglottic larynx, i.e. the arytenoids	Mucosa of hard and soft palate
Caudal	1-2 slices below the appearance of arytenoid cartilages, individually. Thus, the false vocal cords fall within the borders of the structure.	Clinically, it varies from 0 to 1 cm below the free level of the true vocal cord, extending inferiorly from the lateral margin of the ventricle [19; 23]. From practical point of view, the disappearance of the thyroid angle is a good landmark.	<u>Anterior:</u> mylohyoid muscle + anterior belly of the digastric muscle <u>Posterior:</u> root of the tongue and hyoid bone [1]

Table 4. Anatomical borders of the pharyngeal constrictor muscles.

Organ boundaries	**Superior pharyngeal constrictor muscle (SC)**	**Middle pharyngeal constrictor muscle (MC)**	**Inferior pharyngeal constrictor muscle (IC)**
Anterior	Caudal tip of the pterygoid plates [13]	Hyoid bone, root of the tongue [13]	Soft tissue of the larynx [13]
Posterior	Longus capitis and colli muscles[1], i.e. the prevertebral muscles [13; 24]		
Medial	NA/pharyngeal lumen [13]		
Lateral	Medial pterygoid muscle [13], parapharyngeal space	Greater horn of hyoid bone [13]	Superior horn of thyroid cartilage [1; 13]
Cranial	Caudal tip of pterygoid plates[2] [13; 25]	Cranial edge of C3 vertebra [13]	First slice caudal to the caudal edge of hyoid bone [13]
Caudal	Caudal edge of C2 vertebra [13]	Caudal edge of hyoid bone [13; 25]	Caudal edge of arytenoid cartilages [13]

[1] The former muscle stretches between the base of the skull (insertion: basilar part of occipital bone) and the upper cervical vertebrae (origin: transverse processes of third to sixth cervical vertebrae). The latter lies beneath the longus capitis muscle, on the anterior surface of vertebral bodies and can be followed all the way down to the level of upper thoracic vertebrae (origin: bodies of C5 – Th3 vertebrae, insertion: anterior arch of the atlas)

[2] The pterygopharyngeal part of the superior pharyngeal constrictor muscle originates from the lower third of the medial pterygoid plate and its hamulus. Finding the pterygoid process on MRI images may be challenging, therefore CT correlation is advisable.

Table 5. Anatomical borders of the brachial plexus.

Roots	Trunks	Divisions Cords
First, the intervertebral foramina between C_4-C_5 and T_1-T_2 should be identified [14; 34]. Keep in mind that the cervical spinal nerves emerge above their corresponding vertebrae[1]. This is the reason why the fifth cervical spinal nerve is to be found above the fourth cervical vertebra.	The next step is delineating the trunks of the brachial plexus in the scalene hiatus [14; 34]. The anterior and middle scalene muscles may also be contoured for better understanding anatomical relations.	The last two portions of the brachial plexus are defined as the posterior part of the subclavian and axillary neurovascular bundle, below the insertion of the middle scalene muscle and the sternal extremity of the clavicle [14; 35]. A 5 mm paint tool thickness is recommended for the delineation of the OAR [34; 35].Furthermore, a study by Van der Velde et al. suggests to add a margin of 4.7 mm around this BP contour in order to achieve full coverage of OAR and anatomical variants [36].

[1] Unlike the rest of the spinal nerves that leave the spinal canal below their corresponding vertebrae

Table 6. Comparison between T1 and T2 weighted MRI sequences and CT. The visibility of the organs is graded from 1 to 3, where 3 stands for excellent, 2 for average and 1 for poor visibility.

Organ	T1w	T2w	CT	Remarks
Parotid glands	2	3	2	Any diagnostic T2w MRI sequence is eligible for delin content of the glands creates a well-visible contrast with th
Submandibular glands	2	3	2	Similar MRI morphology to the parotid glands.
Mandible	2	2	3	Contouring the mandible on CT is easier, due to the shar bone and the surrounding soft tissues. On T2w MRI the cc intensity layer enveloping the inhomogeneous spongious b
Supraglottic larynx	2	2	2	
Glottic larynx/glottic area	2	2	2	Nonossified cartilages appear with intermediate signal i cartilages are similar to bone, i.e. high signal central marro
Oral cavity	2	2	1	The visibility of the muscles of the floor of the mouth and cranial and caudal border of the region is hard to define. MRI slices beside the axial plane is crucial to correctly d lateral extent of the oral cavity [40].
Pharyngeal constrictor muscles	2	3	1	The constrictor muscles are virtually not distinguishable on
Inner ear	1	2	2	The fluid content of both the cochlea and semicircular images. It is surrounded by a narrow, hypointense zor substance of the bony labyrinth.
Eye (eyeball)	2	3	2	Greater contrast on T2 between the tunics of the eyeball hypointense), fluid (hyperintense) and tissues of the orbit.
Lens	3	3	3	Well visible on T1 and T2 as well.
Optic nerve	3	3	2	
Optic chiasm	3	3	1	
Lacrimal gland	1	2	1	Similar MRI morphology to the parotid and submandibular
Brainstem	3	3	1	The demarcation of the organ from the liquor is clearly vis scans, the nigral substance (SN) appears as a longitudir compared to the neighboring red nucleus and pes peduncu
Spinal cord	2	3	1	We have included only spinal cord proper in the contou practice (i.e. contouring the spinal canal) was performed m and low contrast on native topometric CT scans [42].
Brain	3	3	2	
Pituitary gland	2	2	2	Thin MRI slices (slice thickness: 1 mm) with CT correlati purposes [43].
Thyroid gland	2	2	2	Similar MRI morphology to the parotid and submandibular
Brachial plexus	2	2	1	
Esophagus	2	2	2	Hyperintense to muscle on T2w images [43].
Sum	43	**50**	35	